Cell PRESS
Structure
Resource

High-Affinity Gold Nanoparticle Pin to Label and Localize Histidine-Tagged Protein in Macromolecular Assemblies

Kelsey C. Anthony,[1] Changjiang You,[2] Jacob Piehler,[2,*] and Daniel A. Pomeranz Krummel[1,*]
[1]Department of Biochemistry, Brandeis University, 415 South Street, Waltham, MA 02454, USA
[2]Department of Biology, University of Osnabrück, Barbarastraße 11, Osnabrück 49076, Germany
*Correspondence: piehler@uos.de (J.P.), dapk@brandeis.edu (D.A.P.K.)
http://dx.doi.org/10.1016/j.str.2014.01.007

SUMMARY

There is significant demand for experimental approaches to aid protein localization in electron microscopy micrographs and ultimately in three-dimensional reconstructions of macromolecular assemblies. We report preparation and use of a reagent consisting of tris-nitrilotriacetic a[cid]-NTA) conjugated with a monofunctional gol[d] nan[o] particle ([AuNP]tris-NTA) for site-specific, non-co[valent] labeling of protein termini fused t[o] histidin[e] g (His-tag). Multivalent binding of [tris]-N[TA] to a [His]-tag via complexed Ni(II) ions re[sults] in s[ub]nanomolar affinity and a defined 1:1 sto[ichiometry] cise localization of [AuNP]tris-NTA-labeled [pro]teins by electron microscopy is fur[ther] ensured by [the] reagent's short conformation[ally] re[strict]ed linker. We used [AuNP]tris-NTA to l[o]calize His[-tag]ged proteins in an oligomeric ATP[ase] and in the ba[cte]rial 50S ribosomal subunit. [AuNP]tris-NTA can specifically bind to the target prote[in] in these a[s]semblies and is clearly discern[ible]. Ou[r] labeling reagent should find broad appl[icat]ion no[n]-covalent, site-specific labeling of p[rote]in te[r]mini to p[in]point their location in macromol[ecular] [assem]blies.

INTRODUCTION

Single-particle electron microscopy (EM) is a valuable approach to elucidate the structure of large biological assemblies, particularly if an assembly or one or more of its functional states is refractory to crystallization. Significantly, single-particle cryo-EM density maps of symmetric virus particles and other assemblies have been acquired at resolutions and of such quality where it has been possible to trace a Cα-backbone as well as build models that include protein side chains (Zhang et al., 2010; Grigorieff and Harrison, 2011; Hryc et al., 2011). In the case of the most well-studied asymmetric assembly, the ribosome, resolutions of 4.5–5.5 Å have been reported from particles frozen in vitreous ice (Bai et al., 2013). However, the vast majority of single-particle EM-derived three-dimensional reconstructions of asymmetric biological assemblies are at resolutions much lower t[han] tha[t] the ribosom[e], such as those of the spliceosome (van der [...] et al., 2012). However, even at 5.5 Å r[esolu]tion, α helices [and] β sheets appear as tubes and slabs of [d]ensity, respectively (Muirhead and Perutz, 1963; Pomeranz Krummel et al., 2009). The docking of atomic models determined [u]sing X-ray [c]rystallography, nuclear magnetic resonance, or [h]omology [m]odeling into a low-resolution three-dimensional EM [...]map is error-prone in the absence of positional constraints, especially in the context of a compositionally and [s]tructurally diverse assembly. For this reason, there is significant demand for approaches that aid the localization of subunits in a macromolecular assembly.

A label can aid protein localization optimally if it: (1) binds fast and with high affinity to a specific site on the target protein, thus insuring high occupancy and low nonspecific binding; (2) is unambiguously identifiable; i.e., generates high-contrast image features; (3) is of uniform size, structure, and conformation; and (4) is in proximity to the target protein. A broad range of approaches has been employed to serve as labels to aid localization of protein(s) in EM micrographs, but they have not satisfied the listed criteria for an optimal label. Colloidal gold clusters or nanoparticles (AuNPs) provide excellent contrast for depiction with transmission EM (TEM) and antibodies conjugated with a AuNP have been applied as labels to localize protein(s) (Häcker et al., 2008; Ackerson et al., 2010). However, there are fundamental shortcomings of immunogold labeling for precise localization of individual proteins in macromolecular complexes, including: (1) the large size of antibodies (~10 nm diameter); (2) the spatially undefined, multidisperse attachment of the AuNP to an antibody; and (3) the bivalent binding of the typically used IgG molecule.

To overcome the limitations of such biopolymer-based labeling approaches, several small, purely chemical functional groups have been used for conjugating AuNP with proteins via amine or thiol groups (Büchel et al., 2001; Ackerson et al., 2010). However, these approaches not only suffer from a lack of specificity due to multiple lysine and cysteine residues within macromolecular assemblies; but also compared to noncovalent labeling, these chemical reactions are two to three orders of magnitude slower, thus requiring higher concentrations and longer incubation times, which increase the probability of nonspecific modifications. In an attempt to combine the advantages of a small chemical recognition unit with fast and specific noncovalent interaction, AuNPs conjugated to *mono*-nitrilotriacetic acid (*mono*-NTA) (Figure 1A) have been used to bind proteins via an

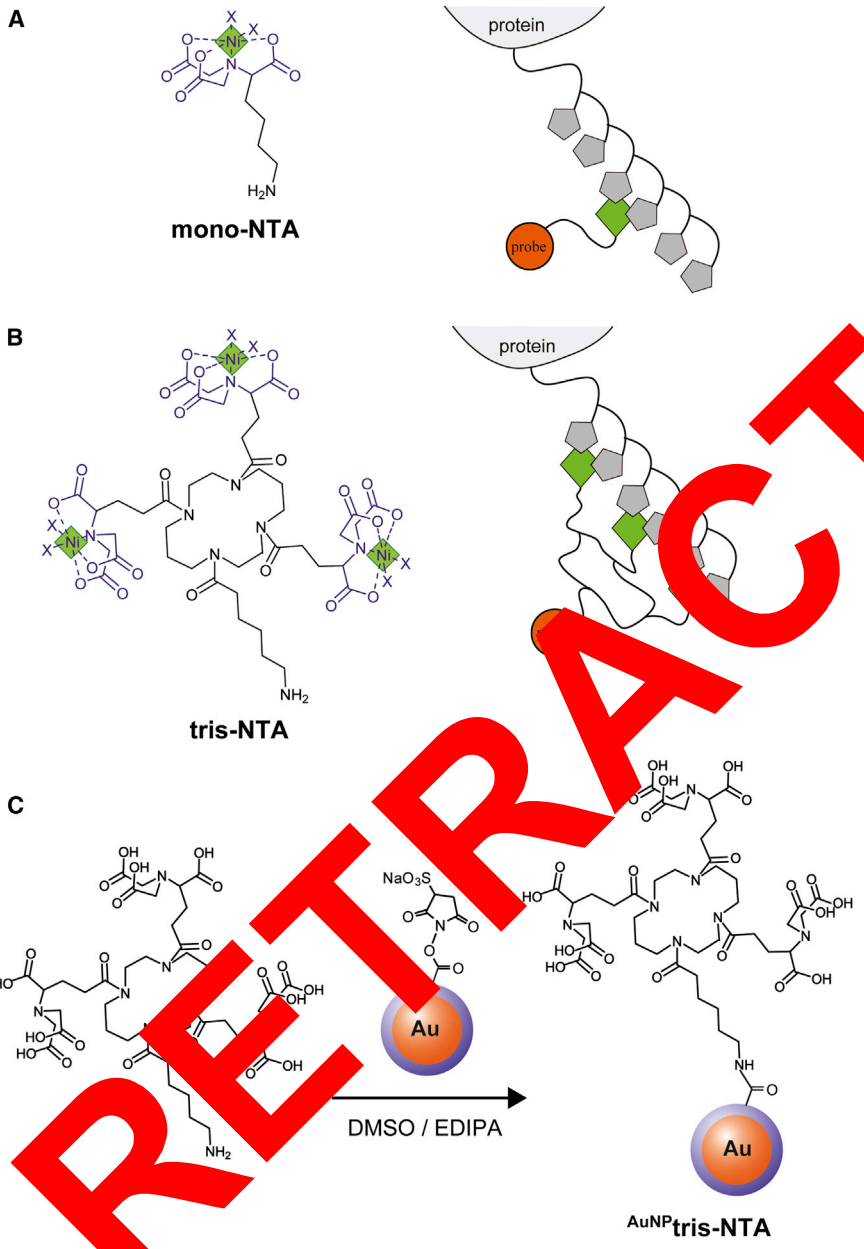

Figure 1. Structure and Preparation of ^{AuNP}tris-NTA

(A) Charged *mono*-nitrilotriacetic acid (NTA; left) and scheme for its binding to a His-tagged protein (right). Complexed ni[illegible]ions are indicated as green diamonds a[illegible] gray pentagons. Ni-NTA posses[illegible]two sites ([illegible]ndicated by an "x") for coord[illegible]n of a His-tag[illegible] protein.

(B) Char[illegible]ed tris[illegible]triacetic ac[illegible]tris-NTA; left) and it[illegible]ding to a [illegible]gged [illegible]in (right). Tris-NT[illegible]s six sites (ea[illegible]d by an "x") for [illegible]ly coor[illegible]ng a His[illegible]ged protein.

[illegible]eac[illegible] of tris-NTA-C_6-NH_2 with *mono*-NHS-Na[illegible] comprisi[illegible] 1.4 nm gold nanocluster (oran[illegible]ated [illegible] an ~0.6 nm phosphine layer (blue) to [illegible]^{AuNP}tris-NTA.

oligohistidine-tag (His-tag; Hainfeld et al., 1999; Hu et al., 2007, 2008). Compared to chemical coupling, capturing via Ni-NTA/His-interaction is much faster (~1 × 10^5 $M^{-1}s^{-1}$), i.e., similar to an antigen-antibody interaction (Lata et al., 2005). However, a drawback to this approach is the low affinity of NTA to a His-tag (~10 μM) due to the fast dissociation rate constant of ~1 s^{-1} of this complex (Lata et al., 2005). Thus, high reagent concentrations are necessary to ensure full labeling and rapid wash-out can be encountered, in the absence of further stabilizing interactions, by proximal amino acid side chains such as cysteine or lysine directly interacting with the AuNP surface. Moreover, the specificity of *mono*-NTA is low because only two histidine residues in close proximity are required for optimum binding (Figure 1A).

[illegible]unctionalization of AuNP with multiple NTA moieties can overcome the problem of low affinity and stability. However, multifunctionalized NTA-AuNP can interact with multiple His-tagged proteins and therefore is prone to promote intermolecular crosslinking. To control the highly desirable multivalent recognition of His-tagged proteins, we designed a molecular entity comprising three NTA moieties grafted onto a cyclic scaffold (tris-NTA) to recognize His-tagged proteins with high affinity and specificity (Figure 1B; Lata et al., 2005). Tris-NTA binds to hexahistidine (H6)-tagged proteins in a 1:1 stoichiometry with ~2 nM affinity and a half-life of several hours, an affinity and half-life four orders of magnitude higher than that of *mono*-NTA (Lata et al., 2005). Because at least six histidine residues in proximity are needed to achieve high-affinity binding, the specificity of tris-NTA toward His-tagged proteins is much higher compared to *mono*-NTA. Whereas proteins having a H6-tag can be efficiently used for labeling, increasing the tag length to a decahistidine (H10)-tag further increases the affinity of the tris-NTA for its target protein to ~0.2 nM (Lata et al., 2005). We have previously used tris-NTA conjugated to fluorescent dyes as well as quantum dots, to efficiently label His-tagged proteins both in vitro and in cell culture (Lata et al., 2006; Reichel et al., 2007; Roullier et al., 2009; You et al., 2010).

Here, we report the conjugation of tris-NTA with a monodisperse gold cluster (^{AuNP}tris-NTA, see Figure 1C) to noncovalently and site-specifically label protein termini genetically fused with a His-tag for the purpose of depiction with TEM. To establish the effectiveness of ^{AuNP}tris-NTA as a label, we used it to determine the location of the His-tagged N terminus of *Thermus thermophilus* (*Tth*) RuvB when it forms an oligomer, in the absence of DNA. *E. coli* RuvB has been reported to assemble into both homo-hexameric (Chen et al., 2002) as well

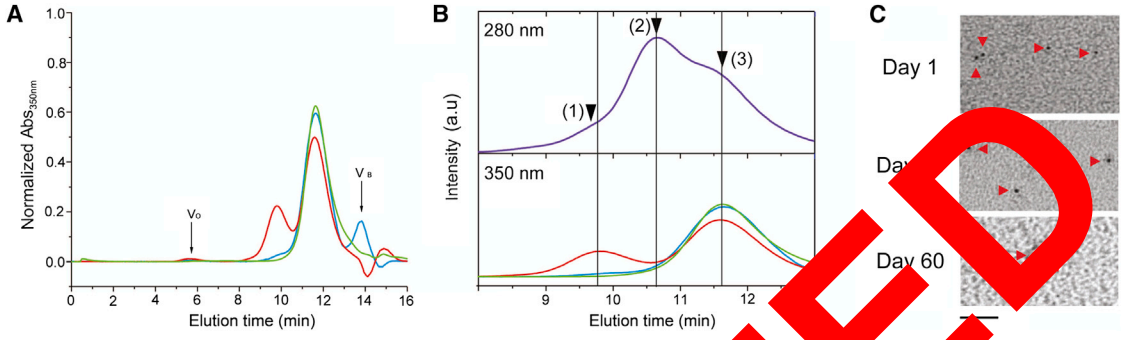

Figure 2. Functional Characterization of ^{AuNP}tris-NTA

(A) Specific binding of ^{AuNP}tris-NTA to a deca-histidine-tagged maltose binding protein (M[illegible]detected with [illegible]ical size exclusion chromatography monitored at 350 nm. Integral intensities of each run were normalized to ^{AuNP}tris-NTA alo[illegible]green [illegible] MBP-H10 incubated with ^{AuNP}tris-NTA (red line); and MBP-H10 incubated with ^{AuNP}tris-NTA in the presence of 10 mM EDTA (blue line). V_o, void volume; V_B, [illegible]volume.

(B) The details of (A; shown in the bottom chromatogram) and a comparison with the [illegible]ogram of MBP-[illegible]ncubated with ^{AuNP}tris-NTA recorded at 280 nm (top chromatogram). The peaks corresponding to MBP-H10 bound to ^{AuNP}tris-N[illegible]1), MBP-H10 (2), and ^{Au}[illegible]tris-NTA (3) are marked by arrows.

(C) ^{AuNP}tris-NTA (8 μM, 1.4 nm diameter AuNP) depicted with TEM after storage[illegible]1, 30, and 60 days. Scale bar, 20 nm. Images acquired using an FEI Morgani TEM operating at 80 keV and 56,000× magnification.

See also Figure S1.

as homo-heptameric rings in the absence of DNA [illegible]d homo-hexamers in the presence of DNA (Miyata[illegible]t al. 2000). We have also used ^{AuNP}tris-NTA to label a single [illegible]t subunit in the large and compositionally [illegible]*E. co*[illegible]S ribosomal subunit, thus challenging the [illegible]agent's [illegible]bility to [illegible]e-cifically and efficiently identify a [illegible]agged [illegible]otein am[illegible]ng a broad array of other protein su[illegible]units. [illegible]ow t[illegible] gold labeling reagent acts as a hig[illegible]finity go[illegible]anoparticle "pin" to label the His-tagged pr[illegible]s in both of [illegible]e challenging assemblies.

RESULTS

^{AuNP}tris-NTA [illegible]epar[illegible]n and Characterization

Specific bindin[illegible]^{AuNP}tris-NT[illegible]to His-tagged proteins was first as[illegible]d by [illegible]lytica[illegible]ze exclusion chromatography (SEC[illegible]sing [illegible] maltos[illegible]ng protein fused with a C-terminal d[illegible]-histidi[illegible]tag (MBP-[illegible]10). ^{AuNP}tris-NTA bound to MBP-H10 w[illegible]oni[illegible]^{AuNP}[illegible]is-NTA's absorption at 350 nm, because the a[illegible]tion cut-off of MBP-H10 is 300 nm (Figure S1A available on[illegible]While ^{AuNP}tris-NTA alone eluted at 11.5 min (Figures 2A and 2B), [illegible]second peak appeared with a retention time of 9.8 min after MBP-H10 was incubated with ^{AuNP}tris-NTA, corresponding to ^{AuNP}tris-NTA bound with MBP-H10. Accordingly, a shoulder around 9.8 min beside the MBP-H10 peak appeared in a SEC trace monitored at 280 nm (Figure S1B). From the intensity ratio of the two peaks, the fraction of functional ^{AuNP}tris-NTA was estimated to be 0.31. As a control for specificity, Ni(II) ions were removed by addition of 10 mM EDTA, reducing the peak of ^{AuNP}tris-NTA bound with MBP-H10 to less than 10% and the sample eluted as ^{AuNP}tris-NTA alone (Figures 2A and 2B). These studies confirmed specific binding of ^{AuNP}tris-NTA to MBP-H10 with high affinity and stability, and with a defined stoichiometry.

^{AuNP}tris-NTA (8 μM) that is not charged with Ni(II) ions appears predominantly monodisperse, as depicted with TEM, when stored at 4°C for up to 60 days (Figure 2C). Over time, however, the ^{AuNP}tris-NTA aggregates to form larger spherical clusters (Figure S1C). Based on the observation that uncharged [illegible]is-NTA was kinetically stable for up to 60 days, the ^{AuNP}tris-NTA was used during this time. Following charging with Ni(II) ions, the ^{AuNP}tris-NTA did not appear to aggregate during the course of our experiments, usually spanning an hour. However, we observed with EM and SEC that after 4 hours following nickel-charging, the colloidal properties of the gold coupled to tris-NTA were destabilized and aggregates were formed. We attribute the aggregation to complexed Ni(II) ions interacting with the surface of another nanoparticle.

Labeling *T. thermophiles* RuvB with ^{AuNP}tris-NTA

To establish utility of the ^{AuNP}tris-NTA to label a macromolecular assembly for depiction with EM, we first explored labeling of the *Thermus thermophiles* (*Tth*) RuvB protein. The *Tth* RuvB used in our studies was fused with an N-terminal deca-histidine-tag (H10) and a three amino acid linker. *Tth* RuvB-H10 overexpressed in *E. coli* and purified to homogeneity retains a His-tag, as demonstrated by staining of the protein on an SDS gel with InVision His-tag stain (Invitrogen; Figure 3A). In the absence of ATP, RuvB-H10 particles do not form clear ring-shaped aggregates (Figure 3B). However, upon addition of ATP, RuvB-H10 oligomers do form ring-shaped oligomers—although not all RuvB-H10 aggregates appear competent to do so (Figure 3B). ^{AuNP}tris-NTA binding in solution may compromise the solubility of RuvB-H10 oligomers and therefore labeling was carried out after RuvB-H10 adsorption to an EM grid. Under these conditions, labeling of RuvB-H10 subunits was highly efficient, with nearly all RuvB-H10 particles that appeared to form rings having five AuNPs bound—as evidenced by examination of particles on the EM grid (Figure 3B). The ^{AuNP}tris-NTA bound to all ring-shaped oligomers present but did not appear to bind to other, non-ring-shaped aggregates. The labeling of RuvB-H10 occurs in a time-dependent manner (Figure 3C). After incubating ^{AuNP}tris-NTA for 20 min, five AuNPs are observed bound per RuvB-H10 oligomer (Figure 3C). Strikingly, each of the five AuNPs bound to the RuvB-H10 oligomer are in similar

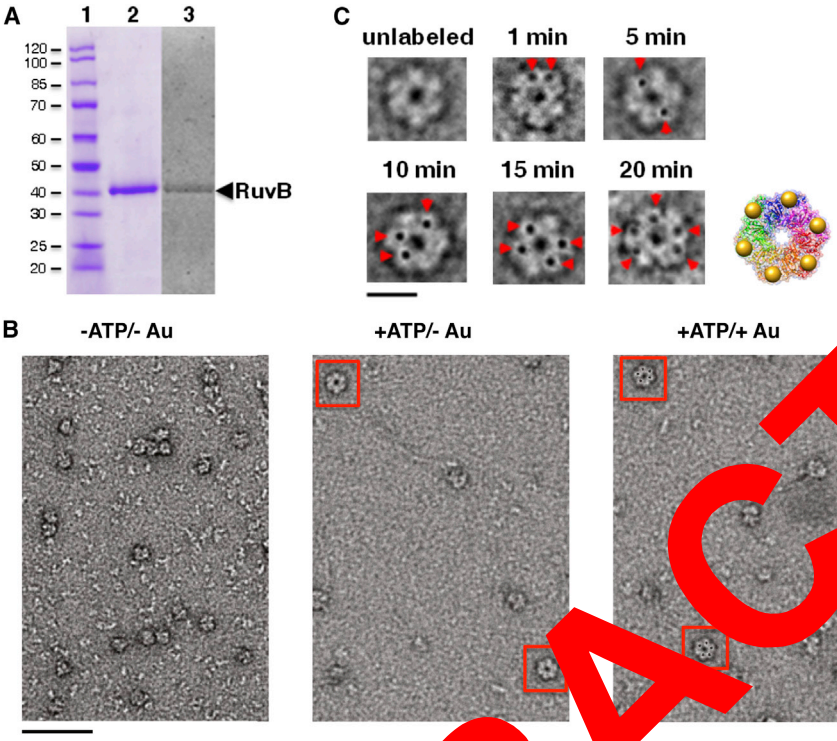

Figure 3. Gold Labeling of Deca-Histidine-Tagged *Thermus thermophiles* RuvB Oligomers with Multivalent ^{AuNP}tris-NTA

(A) Purified deca-histidine-tagged (H10) RuvB electrophoresed on a 12% SDS gel. Shown are a protein molecular weight marker, in kilodaltons (lane 1), purified RuvB-H10 monomer stained with coomassie (lane 2), and RuvB-H10 stained with InVision His-tag stain (lane 3; Invitrogen).

(B) Representative negative-stain EM micrographs of RuvB-H10 in the absence of ATP and unlabeled (left), in the presence of ATP and unlabeled (middle), and in the presence of ATP and labeled with ^{AuNP}tris-NTA (right). Scale bar, 50 nm.

(C) Enlarged images of single RuvB-H10 particles in the presence of ^{AuNP}tris-NTA over time. Gold nanoparticles (AuNPs) are indicated by red arrowheads. Scale bar, 10 nm. A model is shown of a homo-hexameric RuvB-H10 oligomer produced by superposition of six molecules of RuvB-H10 onto the human homo-hexameric oligomer Tip48b (Petukhov et al., 2012). N termini of the monomers are shown bound to AuNP (orange spheres). Monomers of the *Tth* RuvB (Protein Data Bank [PDB] code 1HQC; Yamada et al., 2001) were superimposed individually onto the functionally equivalent domains of the structure of Tip48b (PDB code 3UK6; Petukhov et al., 2012). Superposition was produced using the program MatchMaker and the Needleman-Wunsch alignment algorithm within the Chimera suite of programs (Molecular graphics image of the model was rendered using the UCSF Chimera package (University of California, San Francisco; http://www.cgl.ucsf.edu/chimera). Micrographs acquired using FEI Morgani TEM microscope operating at 80 keV at 45,000× magnification. Sample was stained with 1.5% uranyl acetate.

orientations and equidistant from each other as a result of the short and conformationally restricted linker of the tris-NTA reagent. Incubation times longer than 30 min, however, did not increase the number of AuNPs bound per RuvB-H10 ring. Purified RuvB monomer has been reported to assemble into both homo-heptamer and homo-hexamers in the presence of ATP (Miyata et al., 2000; Iwasaki et al., 2001). One possible explanation as to why we observe only five AuNPs bound per RuvB-H10 ring-shaped oligomer is an inaccessibility of the His-tag of one monomer either due to it being buried or "face down" once adsorbed onto the EM grid and therefore inaccessible for labeling. It is also possible that RuvB-H10 does not form a hexamer efficiently in the absence of DNA. There is no structure of an intact RuvB ring in the absence of DNA. Only crystal structures of a RuvB monomer have been reported, both in a free state and in complex with a RuvA monomer. We, however, produced a model of a RuvB hexamer based on the crystal structure of its human homolog Tip48b, whose hexa-oligomeric structure has been determined (Petukhov et al., 2012). The AuNP labels on RuvB-H10 nicely approximate the more extended N terminus of Tip48b monomers (Figure 3C).

Labeling the *E. coli* 50S Ribosomal Subunit with ^{AuNP}tris-NTA

In addition to labeling *Tth* RuvB-H10, we explored the binding of ^{AuNP}tris-NTA to the *E. coli* 50S ribosomal subunit—a particle significantly more compositionally diverse than RuvB. Overexpression of the human 50S ribosomal subunit Rpl3 protein fused with an N-terminal H10 in *E. coli* yielded a 50S-H10 subunit that contained Rpl3-H10 protein in place of its endogenous bacterial homolog, L3, (Figure 4A) and migrated on a native polyacrylamide gel as an intact complex free of the smaller 30S subunit (Figure 4B). In contrast to the method used to successfully label RuvB-H10, the 50S-H10 subunit could be labeled with ^{AuNP}tris-NTA not only by first absorbing it onto a grid, but also by incubating it with ^{AuNP}tris-NTA in solution and subsequently absorbing the complex onto an EM grid. Our initial observations indicated that a subset of 50S-H10 particles had two AuNPs bound per particle (Figure S2A), which is not consistent with the known stoichiometry of the protein L3. We therefore took several precautions in labeling of the 50S-H10 subunit: (1) its pretreatment with 2-iodoacetamide to alkylate free cysteines; and (2) conducting postlabeling washes of the EM grid with up to 50 mM imidazole in a wash buffer so as to remove non-specific binding of ^{AuNP}tris-NTA to histidine-rich 50S ribosomal protein subunits. We incubated the bacterial 50S sample that was alkylated with iodoacetamide but lacked the His-tagged protein and did not observe nonspecific binding of Au to the 50S when treated with the ^{AuNP}tris-NTA (Figures S2B and S2C). We observed, however, that alkylated 50S-H10 particles bound only single AuNPs and that these bound AuNPs were not dislodged when the labeled sample was washed with up to 50 mM imidazole—single electron dense AuNPs appeared evident when compared to the 50S-H10 subunit not incubated with ^{AuNP}tris-NTA (Figure 4C). Not all 50S-H10 particles were labeled with a ^{AuNP}tris-NTA, as one would expect if the 50S-H10 particles adsorbed to an EM grid without a significant bias in orientation. In addition, not all 50S-H10 particles may

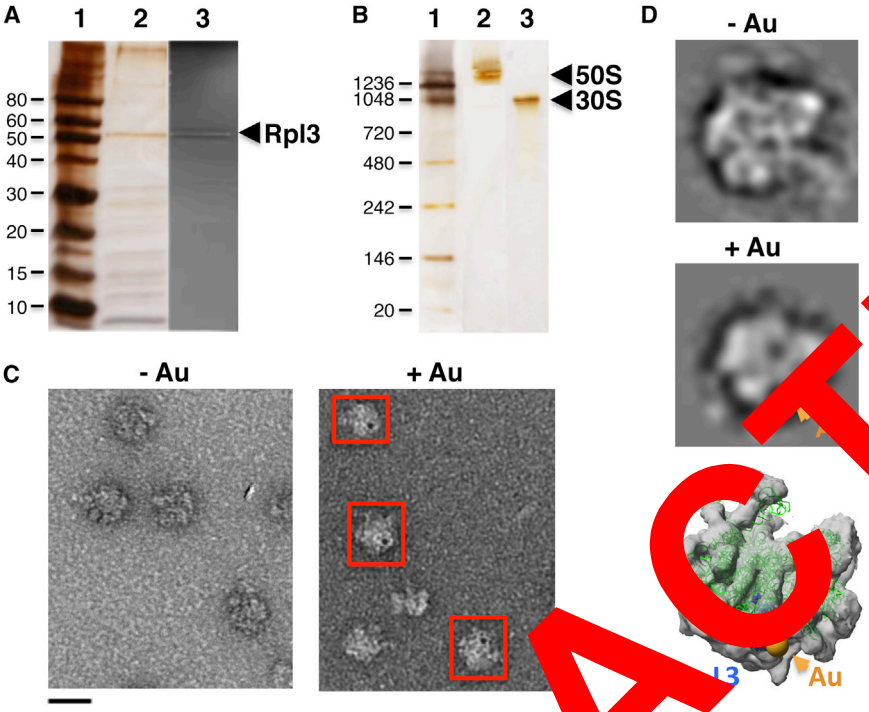

Figure 4. Labeling of *Escherichia coli* 50S Ribosomal Subunit with ^{AuNP}tris-NTA

(A) Purified *E. coli* 50S subunit containing the deca-His-tagged (H10) protein Rpl3 (50S-H10) electrophoresed on a 12% SDS gel. Shown are a protein molecular weight ladder, in kilodaltons (lane 1); *E. coli* 50S-H10 silver stained (lane 2); and *E. coli* 50S stained with Invitrogen His-tag stain (Invitrogen), highlighting the presence of Rpl3-H10 (lane 3).

(B) Purified *E. coli* 50S subunit electrophoresed on a native polyacrylamide gradient (3%–12%) gel and silver stained. Shown are a molecular weight ladder in kilodaltons (lane 1); purified *E. coli* 50S subunit (lane 2); and purified *E. coli* 30S subunit.

(C) Raw EM micrographs showing a lawn of negative-stained *E. coli* 50S-H10 particles not incubated with ^{AuNP}tris-NTA and *E. coli* 50S-H10 particles incubated with the ^{AuNP}tris-NTA. 50S-H10 particles in complex with AuNPs are boxed in red. Scale bar, 20 nm.

(D) Selected class averages of unlabeled 50S-H10 and of the 50S-H10 labeled with ^{AuNP}trisNTA. Shown is a crystal structure of the *E. coli* 50S subunit (green; PDB code 3R8S; Dunkle et al., 2011) with the exception of L3, which is colored blue with its N terminus shown bound to a 1.4 nm diameter sphere (orange) to represent the gold nanoparticle. The crystal structure is fitted into the envelope (EMD code 1019; Matadeen et al., 1999).

Images for (C) acquired using an FEI Morgani TEM at 80 keV at 36,000× magnification. Data for preparation of class averages shown in (D) were collected on a Phillips CM12 operating at 100 keV at 45,000× magnification. Sample negative-stained with 1.5% uranyl acetate. The molecular graphics image was rendered using the UCSF Chimera package (University of California, San Francisco; http://www.cgl.ucsf.edu/chimera). See also Figure S2.

have the larger human Rpl3-H10 in place of the endogenous bacterial protein homolog L3. Indeed, the replacement of an exogenously overexpressed protein for the endogenous variant in the ribosome has been shown to be protein-dependent and yield a successful incorporation of 25%–50% (Uhlein et al., 1998). It is not critical, however, that all 50S particles contain the exogenous tagged protein for the purpose of localization. Of course, it is important that the protein binds stoichiometrically to the correct site on the 50S and that the AuNP recognizes and binds to only this protein. To highlight the success of AuNP labeling of the human protein Rpl3-H10 incorporated into the bacterial 50S, we selected those particles with the AuNP bound and generated two-dimensional classifications of these 50S-H10 particles (Figure 4D). As shown in a class average, the AuNP is clearly apparent as a distinct dense body—absent in the class average of the same view of 50S-H10. Importantly, the AuNP position reliably colocalized with the site of the *E.coli* L3 protein (Figure 4D), confirming the high targeting fidelity of ^{AuNP}tris-NTA.

DISCUSSION

We introduced tris-NTA conjugated with a monodisperse 1.4 nm diameter gold nanoparticle, present in a 1:1 ratio, as a powerful tool for localization of His-tagged proteins within macromolecular assemblies studied with EM. Tris-NTA is attractive as a scaffold for labeling because it has a subnanomolar affinity and defined 1:1 stoichiometry for a His-tag, thus ensuring fast binding and high specificity for its "target" protein and low nonspecific binding. Compared to protein-based recognition, tris-NTA is a very small compound—we therefore expected that it would bring the AuNP in proximity to a "target" protein's terminus to accurately pinpoint its location. We successfully used ^{AuNP}tris-NTA to localize His-tagged proteins in the *T. thermophiles* ATPase RuvB and in the *E. coli* 50S ribosomal subunit. Efficient labeling with ^{AuNP}tris-NTA was possible both in solution and after particle adsorption onto an EM grid. Yet as we observed for RuvB, the binding of multiple ^{AuNP}tris-NTA to a single protein complex in solution may affect macromolecular solubility. The order of labeling and adsorbing one's sample onto an EM grid is thus a point to consider in optimizing the labeling strategy of a particle. Moreover, nonspecific binding of the AuNP to cysteine residues has to be considered as a potential side reaction, which can be blocked by alkylation prior to the labeling reaction. We also washed the ribosomal 50S-H10 subunit with imidazole at a concentration as high as 50 mM to ensure that the ^{AuNP}tris-NTA did not complex with unintended histidine-rich protein(s). Following the pre- and postlabeling treatment and wash of the ribosomal 50S-H10 subunit, we obtained particles that had only a single AuNP bound. Class averages of the AuNP labeled 50S-H10 indicated the location of the His-tagged protein L3.

Exhibiting rapid, site-specific labeling with high affinity, specificity, and defined stoichiometry in combination with its small size, the ^{AuNP}tris-NTA reagent ideally fulfills the requirements for precisely pinpointing protein termini in macromolecular assemblies by EM. We applied ^{AuNP}tris-NTA after protein adsorption to an EM grid as relatively fragile assemblies were

involved. However, purification of protein complexes after incubation with ^{AuNP}tris-NTA as demonstrated for MBP-H10 and 50S-H10 is also possible, opening exciting possibilities for cryo-EM applications, which has been shown to be compatible with such 1.4 nm AuNP. Thus, we believe that ^{AuNP}tris-NTA should find broad application in noncovalent, site-specific labeling of protein termini to pinpoint their location in macromolecular assemblies as well as in challenging applications such as in situ electron tomography that requires protein localization in a complex and crowded milieu. We also envision other possible roles for the ^{AuNP}tris-NTA once bound to its intended target, including serving as a fiducial marker by providing high-contrast image features for particle identification in vitrified ice and aiding particle classification and/or alignment (Jensen and Kornberg, 1998).

EXPERIMENTAL PROCEDURES

Conjugation of tris-NTA with a Monofunctional Gold Nanoparticle

Tris-NTA modified by an aminocaproic acid (tris-NTA-C_6-NH_2, 1046 Da) was synthesized as previously described (Lata et al., 2005). The overall synthesis of ^{AuNP}tris-NTA is outlined in Figure 1C. One milligram of the tris-NTA-C_6-NH_2 was dissolved in 100 µl dry dimethyl sulfoxide (DMSO) con… ethyldiisopropylamine. Six nmoles of *mono*-Sulfo-N-hydroxy-Suc… Nanogold (*mono*-NHS-Nanogold, 1.4 nm diameter; Nanoprobes) … dissolved in 100 µl dry DMSO and then suspended in a 2 ml glass reacto… reaction at room temperature for 20 hr under N_2 … in the … 100 µl water was added for 30 min to quench th… S es… The mi… was subsequently loaded onto a 2 ml NAP-5 c… n (G25… A grade; Healthcare) for purification. The relevant frac… wer… … to approximately 150 µl using an Amicon Ult… centri… (Ultracel… 5 ml, 10,000 MWCO). The sample was the… ashed thre… es with 500 µl of 20 mM HEPES (4-(2-hydroxyethyl)… razineethanes… acid), pH 7.5 to further remove the un-coupled … mpounds. The … nanoparticle concentration was determined b… UV-Vis… trometric reading at 420 nm, applying an extinction coef… nt of 156,000 … $^{-1}$ from the manufacturer. A typical yield of 36% h… on the total *mono*-N… Nanogold was obtained from the preparation… hout lo… with nickel(II) ions, ^{AuNP}tris-NTA can be stored at 4°C for a… 2 m… in 20 mM HEPES, pH 7.5.

Nickel loading was … cording t… eviously published protocol with modificatio… et al… 0). In … for labeling of the RuvB-H10 and 50S-H1… … µl of … tris-NTA stock solution was mixed with 100 … nM and … 0 µl 100 … $NiCl_2$, respectively, in 20 mM HEPES, pH 7.5 … min, … … onto an Amicon Ultra centrifugal filter (Ultracel, 0.5 m… … as centrifuged at 10,000 revolutions per minute for 5 min. … ample was buffer exchanged on the concentrator with addition of 900 µl … S to remove residual nickel ions. The ^{AuNP}tris-NTA was then immediate… thin 1 hr) used for protein labeling at a concentration of 500 nM.

Functional Characterization of ^{AuNP}tris-NTA

Specific interaction of ^{AuNP}tris-NTA with His-tagged proteins in solution was explored by SEC using maltose binding protein with a C-terminal deca-histidine-tag (MBP-H10) as a model protein. Labeling was done according to a previously published protocol (You et al., 2010). The freshly prepared Ni(II)-loaded ^{AuNP}tris-NTA was incubated with MBP-H10 in HEPES buffered saline (HBS) for 30 min with final concentrations of ^{AuNP}tris-NTA and MBP-H10 at approximately 100 nM and 3 µM, respectively. The sample was fractionated by a Superdex 200 5/150 SEC column (GE Healthcare) using a high-pressure liquid chromatography (HPLC) system (Jasco) monitored by a diode array detector (MD-2015 plus; Jasco) at a flow rate of 0.2 ml/min.

Preparation of *Tth* RuvB and the *E. coli* 50S Ribosomal Subunit

The *Thermus thermophiles* (*Tth*) RuvB gene coding for full-length RuvB protein (324 residues; 37 kDa) was cloned into the pET3a expression vector (QIAGEN). *Tth* RuvB was cloned with an N-terminal deca-histidine-tag (H10) followed by a three amino acid (Ser-Ser-Gly) linker. BL21 (DE3) cells transformed with RuvB-H10 were grown in Luria Broth (LB) at 37°C. Cells were induced with 1 mM isopropyl β-D-1-thiogalactopyranoside (IPTG) at an optical density 600 (OD_{600}) of 0.8 and grown for 5 hr postind… at 37°C. Cells were harvested by centrifugation at 5,000 rpm fo… C. The cell pellet was suspended and cells lysed in 20 m… HEPES, p… 0.5 M NaCl; 50 mM imidazole, with EDTA-free protea… ibitor cockta… che) present. Soluble fraction(s) were heated at 75°C for … and placed … °C for 30 min to denature and precipitate n… rmophili… teins. … ethyleneimine (0.01% final concentration) w… ded to the rem… ble protein while mixing on ice for 1 hr to … ve DN… approa… scribed previously (Burgess, 1991). DNA was … pelle… and the remaining protein was loaded onto a gravity colum… otain… A resin (Q… EN) for affinity purification of full-length Ru… 10. Protei… elut… using a linear gradient from 0-500 mM imi… in 20 mM HE… .5; 0.5 M NaCl. RuvB-H10 was further purifi… and… r exchanged … a storage buffer (20 mM tris-HCl, pH 7.8; 0.2 M KCl) by … using a Superdex 200 16/60 column (GE Healthcare). Purified protein was … at 4°C. To assemble RuvB-H10 in the absence of … ified RuvB-H10 … µM was incubated with 2 mM ATP/10 mM … l_2 for 30 min at 37°C, as described previously (Tong and Wetmur, 1996). … he gene codi… or full-length human 60S ribosomal subunit protein Rpl3 … residues; 46… a) was cloned into the pET15b expression vector, such t… natural i… or methionine position is preceded by a deca-histidine-tag, … linker, and a thrombin cleavage site (Kelly et al., 2008; gift of Dukov… and Walz). Rpl3-H10 is the human homolog of *E. coli* 50S ribosomal subunit protein L3. Rpl3-H10 was overexpressed in *E. coli* BL21 (DE3) … ntially as previously described (Kelly et al., 2008). BL21 (DE3) cells transformed with Rpl3-H10 were grown in LB at 37°C. Cells were induced with 0.5 mM IPTG at OD_{600} = 0.8 and grown overnight at 16°C. The cells were harvested by centrifugation at 5,000 rpm for 20 min at 4°C. The cell pellet was suspended in ribosomal buffer (20 mM HEPES-K, pH 7.5; 6 mM magnesium acetate; 30 mM ammonium acetate; 4 mM β-mercaptoethanol [BME]) and centrifuged at 4,000 rpm for 20 min at 2°C. The cell pellet was flash-frozen in liquid nitrogen and stored at −80°C. Cells were lysed using a bead-beater and aluminum oxide. Lysed cells were centrifuged for 15 min at 12,300 rpm followed by centrifugation at 17,600 rpm for 55 min at 2°C. The supernatant was centrifuged for an additional 18 hr at 2°C and 40,700 rpm. The top layer was removed from the pellet, while the bottom layer was rinsed with and suspended in dissociation buffer (20 mM HEPES-K, pH 7.5; 1 mM magnesium acetate; 200 mM ammonium acetate; 4 mM BME). The sample was centrifuged at 14,000 rpm for 15 min at 2°C to pellet insoluble aggregate. Approximately 150 OD_{260} units of sample were layered onto a 10%–30% sucrose gradient prepared with ribosomal dissociation buffer. Gradients were centrifuged at 19,000 rpm for 17 hr at 2°C. Each gradient was fractionated by pipetting 1 ml fractions starting at the top of the gradient until the bottom was reached. Every second fraction was run on a 1.2% agarose gel. Fractions containing 50S-H10 ribosomal RNA were pooled and 10% of the total volume of dissociation buffer was added. 50S-H10 subunit fractions were centrifuged at 70,000 rpm at 2°C for 24 hr to pellet the 50S-H10 ribosomal subunit. 50S-H10 subunit pellets were then suspended in dissociation buffer. Purified 50S-H10 subunit was flash frozen in liquid nitrogen and stored at −80°C until use.

Depiction of Unlabeled *Tth* RuvB and the *E. coli* 50S Ribosomal Subunit

Approximately 4 µl of either 5 µM *Tth* RuvB-H10 or *E. coli* 50S with or without Rpl3-H10 were applied to glow-discharged carbon-coated copper 400 mesh EM grids (SPI Supplies). Samples were incubated on the grid for 1 min and then blotted using filter paper. Grids with bound RuvB-H10 or *E. coli* 50S subunit variants were washed once to remove aggregates with either RuvB-H10 storage buffer or ribosomal dissociation buffer, respectively. Grids were negatively stained by addition of three drops of 1.5% uranyl acetate, blotting between drops. Grids were dried for at least 5 min prior to depiction using an FEI Morgani TEM operating at 80 keV or a Phillips CM12 operating at 120 keV.

Labeling of *Tth* RuvB and *E. coli* 50S Subunit with ^{AuNP}tris-NTA

The ^{AuNP}tris-NTA was demonstrated in the absence of substrate by dispensing 4 µl of the charged label (500 nM) onto a glow-discharged copper-coated

400 mesh EM grid, allowing the sample to dry, staining the grid with 1.5% uranyl acetate, and then depicted with TEM as described above. To label RuvB-H10, the purified and assembled complex was similarly applied to glow-discharged carbon-coated EM grids at 5 μM. Grids were washed once with RuvB-H10 storage buffer and blotted. Subsequently, 4 μl of charged ^{AuNP}tris-NTA (500 nM) was dispensed onto the grid containing the washed sample and incubated for 1, 5, 10, 15, or 20 min. Following, grids were washed twice with RuvB-H10 storage buffer and blotted to remove unbound ^{AuNP}tris-NTA. Labeled RuvB-H10 was then stained with 1.5% uranyl acetate and depicted with TEM, as described above for the unlabeled complex.

To label *E. coli* 50S-H10 subunit, purified sample was either labeled directly in solution or first alkylated to prevent thiol-mediated interaction with the AuNP. To alkylate the 50S-H10 subunit, 4 μl of 5 OD_{260} units of 50S-H10 subunit was incubated with 1 μl 15 mM 2-Iodoacetamide (5 mM final) for 15 min and then buffer exchanged to remove free 2-Iodoacetamide. *E. coli* 50S-H10 subunit was then labeled either on a grid or in solution by incubation with 500 nM charged ^{AuNP}tris-NTA and incubation for 1 to 3 min. Labeled 50S-H10 was applied to the grid for 1 min and then blotted using filter paper. Grids were washed twice with ribosomal dissociation buffer containing 20-50 mM imidazole to remove possible non-specific interactions of the ^{AuNP}tris-NTA and sample. Between washes, grids were blotted to remove any aggregate and unbound ^{AuNP}tris-NTA. Labeled 50S-H10 subunit was then stained with 1.5% uranyl acetate and visualized by TEM, as described above for the unlabeled particle.

Preparation of *E. coli* 50S Class Averages

Grids were prepared of *E. coli* 50S-H10 ribosomal subunits con[illegible]ing the deca-His-tagged Rpl3, with or without bound ^{AuNP}tris-NTA - as [illegible]rib above. Data for preparation of class averages were [illegible]ted on a [illegible]s CM12 operating at 120 keV at 31,000× magnifi[illegible]n, [illegible]2,036 a[illegible]17 particles were picked for the unlabeled and [illegible]ris-NTA [illegible]beled 50S [illegible]0 subunits, respectively, using e2boxer (Tang [illegible]2007) [illegible]-H10 part[illegible]les class averages were produced and further refi[illegible]the [illegible]mage processing software package (van H[illegible]et al., 199[illegible]

SUPPLEMENTAL INFORMA[illegible]N

Supplemental Informat[illegible]ncludes two figu[illegible]nd can be found with this article online at http[illegible]doi.org/10.1016/j.str.2[illegible].01.007.

ACKNOWLEDGM[illegible]

This w[illegible]upporte[illegible]National Science Foundation Materials Res[illegible]h Scie[illegible]and Engi[illegible]g Center at Brandeis (to D.A.P.K.), an inves-t[illegible] grant fr[illegible]the National Science Foundation (to D.A.P.K.; award number 11[illegible]), the Deutsche Forschungsgemeinschaft (to J.P.; SFB9[illegible]). We are grateful to Nikolaus Grigorieff for advice and support, Tom Walz and [illegible]iela Dukovski for the His-tagged Rpl3 clone, Axel Brilot for guidance in [illegible]ration of the *E. coli* 50S ribosomal subunit, Clarisse van der Feltz and Mike Rigney for discussion, and Chen Xu for EM guidance and advice. D.A.P.K. is very grateful for the inspiration during the later stages of this work provided by Amita Sarai Pomeranz, a "golden girl". The Brandeis EM facility is supported by National Institutes of Health grant P01 GM62580.

Received: April 18, 2013
Revised: January 8, 2014
Accepted: January 16, 2014
Published: February 20, 2014

REFERENCES

Ackerson, C.J., Powell, R.D., and Hainfeld, J.F. (2010). Site-specific biomolecule labeling with gold clusters. Methods Enzymol. *481*, 195–230.

Bai, X.-C., Fernandez, I.S., McMullan, G., and Scheres, S.H. (2013). Ribosome structures to near-atomic resolution from thirty thousand cryo-EM particles. eLife *2*, e00461.

Büchel, C., Morris, E., Orlova, E., and Barber, J. (2001). Localisation of the PsbH subunit in photosystem II: a new approach using labelling of His-tags with a Ni$^{(2+)}$-NTA gold cluster and single particle analysis. J. Mol. Biol. *312*, 371–379.

Burgess, R.R. (1991). Use of polyethyleneimi[illegible]ification of DNA-binding proteins. Methods Enzymol. *208*, 3–10.

Chen, Y.-J., Yu, X., and Egelman, E.H. [illegible]2). The hexam[illegible]ring structure of the Escherichia coli RuvB branch migrati[illegible]otein. J. Mol. [illegible]. *319*, 587–591.

Dunkle, J.A., Wang, L., Feldm[illegible]M.B., Pu[illegible] Chen[illegible]., Kapral, G.J., Noeske, J., Richardson, J[illegible] Blanchard, S[illegible]ate, J.H. (2011). Structures of the bacteri[illegible]osome[illegible]lassical[illegible]ybrid states of tRNA binding. Science *332*, 9[illegible]4.

Grigorieff, N., and [illegible]rison, [illegible]2011). Ne[illegible]omic resolution reconstructions of icosah[illegible]al viruses [illegible]elect[illegible]cryo-microscopy. Curr. Opin. Struct. Biol. [illegible]–273.

Häcker, [illegible]ander[illegible]Golas, M.M., Wolf, E., Karagöz, E., Kastner, B., Stark, H., Fabrizio, P., and [illegible]mann, R. (2008). Localization of Prp8, Brr2, Snu114 and [illegible]6 proteins in [illegible]east tri-snRNP by electron microscopy. Nat. [illegible]ol. Biol. *15*, 1206–[illegible]12.

[illegible]ainfeld, J.F., Li[illegible] W., Halsey, C.M., Freimuth, P., and Powell, R.D. (1999). [illegible]i-NTA-gold c[illegible]rs target His-tagged proteins. J. Struct. Biol. *127*, 185–198.

[illegible]. C.F., Che[illegible].H., and Chiu, W. (2011). Near-atomic-resolution cryo-EM f[illegible]ulo[illegible]logy. Curr Opin Virol *1*, 110–117.

Hu, M., Qian, L., Briñas, R.P., Lymar, E.S., and Hainfeld, J.F. (2007). Assembly of nanoparticle-protein binding complexes: from monomers to ordered arrays. [illegible]. Chem. Int. Ed. Engl. *46*, 5111–5114.

Hu, M., Qian, L., Briñas, R.P., Lymar, E.S., Kuznetsova, L., and Hainfeld, J.F. (2008). Gold nanoparticle-protein arrays improve resolution for cryo-electron microscopy. J. Struct. Biol. *161*, 83–91.

Jensen, G.J., and Kornberg, R.D. (1998). Single-particle selection and alignment with heavy atom cluster-antibody conjugates. Proc. Natl. Acad. Sci. USA *95*, 9262–9267.

Kelly, D.F., Dukovski, D., and Walz, T. (2008). Monolayer purification: a rapid method for isolating protein complexes for single-particle electron microscopy. Proc. Natl. Acad. Sci. USA *105*, 4703–4708.

Lata, S., Reichel, A., Brock, R., Tampé, R., and Piehler, J. (2005). High-affinity adaptors for switchable recognition of histidine-tagged proteins. J. Am. Chem. Soc. *127*, 10205–10215.

Lata, S., Gavutis, M., Tampé, R., and Piehler, J. (2006). Specific and stable fluorescence labeling of histidine-tagged proteins for dissecting multi-protein complex formation. J. Am. Chem. Soc. *128*, 2365–2372.

Matadeen, R., Patwardhan, A., Gowen, B., Orlova, E.V., Pape, T., Cuff, M., Mueller, F., Brimacombe, R., and van Heel, M. (1999). The Escherichia coli large ribosomal subunit at 7.5 A resolution. Structure *7*, 1575–1583.

Miyata, T., Yamada, K., Iwasaki, H., Shinagawa, H., Morikawa, K., and Mayanagi, K. (2000). Two different oligomeric states of the RuvB branch migration motor protein as revealed by electron microscopy. J. Struct. Biol. *131*, 83–89.

Muirhead, H., and Perutz, M.F. (1963). Structure of Haemoglobin. A three-dimensional fourier synthesis of reduced human Haemoglobin at 5.5 Å resolution. Nature *199*, 633–638.

Petukhov, M., Dagkessamanskaja, A., Bommer, M., Barrett, T., Tsaneva, I., Yakimov, A., Quéval, R., Shvetsov, A., Khodorkovskiy, M., Käs, E., and Grigoriev, M. (2012). Large-scale conformational flexibility determines the properties of AAA+ TIP49 ATPases. Structure *20*, 1321–1331.

Pomeranz Krummel, D.A., Oubridge, C., Leung, A.K.W., Li, J., and Nagai, K. (2009). Crystal structure of human spliceosomal U1 snRNP at 5.5 Å resolution. Nature *458*, 475–480.

Reichel, A., Schaible, D., Al Furoukh, N., Cohen, M., Schreiber, G., and Piehler, J. (2007). Noncovalent, site-specific biotinylation of histidine-tagged proteins. Anal. Chem. *79*, 8590–8600.

Roullier, V., Clarke, S., You, C., Pinaud, F., Gouzer, G.G., Schaible, D., Marchi-Artzner, V., Piehler, J., and Dahan, M. (2009). High-affinity labeling and tracking

of individual histidine-tagged proteins in live cells using Ni^{2+} tris-nitrilotriacetic acid quantum dot conjugates. Nano Lett. *9*, 1228–1234.

Tang, G., Peng, L., Baldwin, P.R., Mann, D.S., Jiang, W., Rees, I., and Ludtke, S.J. (2007). EMAN2: an extensible image processing suite for electron microscopy. J. Struct. Biol. *157*, 38–46.

Tong, J., and Wetmur, J.G. (1996). Cloning, sequencing, and expression of ruvB and characterization of RuvB proteins from two distantly related thermophilic eubacteria. J. Bacteriol. *178*, 2695–2700.

Uhlein, M., Weglöhner, W., Urlaub, H., and Wittmann-Liebold, B. (1998). Functional implications of ribosomal protein L2 in protein biosynthesis as shown by in vivo replacement studies. Biochem. J. *331*, 423–430.

van der Feltz, C., Anthony, K., Brilot, A., and Pomeranz Krummel, D.A. (2012). Architecture of the spliceosome. Biochemistry *51*, 3321–3333.

van Heel, M., Harauz, G., Orlova, E.V., Schmidt, R., and Schatz, M. (1996). A new generation of the IMAGIC image processing system. J. Struct. Biol. *116*, 17–24.

Yamada, K., Kunishima, N., Mayanagi, K., Ohnishi, T., Nishino, T., Iwasaki, H., Shinagawa, H., and Morikawa, K. (2001). Cry[illegible]ture of the Holliday junction migration motor protein RuvB fr[illegible]*rmophilus* HB8. Proc. Natl. Acad. Sci. USA *98*, 1442–144[illegible]

You, C., Wilmes, S., Beutel, O., Löchte, S., [illegible]lelowa, Y., [illegible]r, F., Richter, C., Seine, T., Schaible, D., Uzé, G. [illegible]. (2010). [illegible]-controll[illegible]nofunctionalization of quantum dots for m[illegible]exed protein[illegible]ve cells. Angew. Chem. Int. Ed. Engl. *49*, 410[illegible]12.

Zhang, J., Baker, M.L., Sch[illegible] G.F., [illegible]ouglas, N.R., Reissmann, S., Jakana, J., Dougherty, M., Fu[illegible], Le[illegible] Ludtke, S. [illegible]et al. (2010). Mechanism of folding chamber c[illegible]re in a gro[illegible]shape[illegible]. Nature *463*, 379–383.